LA-UR -85-933

CONF-850801--15

Los Alamos National Laboratory is operated by the University of California for the United States Department of Energy under contract W-7405-ENG-36.

LA-UR--85-933

DE85 010109

TITLE: SEISMIC STUDIES OF A MASSIVE HYDRAULIC FRACTURING EXPERIMENT

AUTHOR(S): Leigh House, Hans Keppler, and Hideshi Kaieda

SUBMITTED TO: Geothermal Resources Council, 1985 meeting
Kailua-Kona, Hawaii, August 26-30, 1985

DISCLAIMER

Los Alamos Los Alamos National Laboratory
Los Alamos, New Mexico 87545

FORM NO. 836 R4
ST. NO. 2629 5/81

DISCLAIMER

SEISMIC STUDIES OF A MASSIVE HYDRAULIC FRACTURING EXPERIMENT

Leigh House, Hans Keppler[1], and Hideshi Kaieda[2]

Earth and Spaces Sciences Division, Los Alamos National Laboratory, Los Alamos, NM 87545
[1]Visiting Scientist, Federal Institute for Geosciences and Natural Resources (BGR), Hannover, Germany,
[2]Visiting Scientist, Central Research Institute of Electric Power Industry, Chiba, Japan

ABSTRACT

During a massive hydraulic fracturing experiment carried out at Fenton Hill, New Mexico, 850 microearthquakes, ranging in magnitudes from -3 to 0, were located reliably using arrival times recorded at a set of 5 downhole geophone stations. A subset of these events were located using an upgraded hodogram technique. The seismicity defines a tabular zone with horizontal extent of 900 m, vertical extent of 800 m, and thickness of 150 m. This zone strikes N340°E, and dips 75° to the east; its position indicates that no hydraulic connection between the two predrilled wells could be achieved by the fracturing. The distribution of locations obtained from arrival times shows good agreement with those derived from hodograms. Well constrained fault plane solutions were determined for 26 of the larger microearthquakes observed at a surface seismic net. Most solutions display one nearly vertical nodal plane that strikes close to N - S, and a T axis that trends roughly E - W, in agreement with regional indicators of the least principal stress direction.

INTRODUCTION

In December, 1983, a hydraulic fracturing experiment (termed experiment 2032) was carried out at the Fenton Hill Hot Dry Rock site, New Mexico. A total of 21,330 m^3 (5.6×10^6 gallons) of water were injected into a 20 m long open-hole interval at a depth of 3,500 m into the lower of two inclined wells, EE-2. Injection proceeded for about 60 hours, at an average wellhead pressure of 48 MPa (7000 psi) and injection rate of 0.1 m^3/s (40 barrels/min). Fluid injection was abruptly terminated by a tubing failure at the wellhead, after which the injection well vented back heated fluid and steam. Seismic monitoring began shortly after the start of injection, and continued for about 24 hours after the onset of venting.

Downhole monitoring of induced seismicity consisted of three triaxial geophone tools, all located within a few hundreds of meters of the seismic activity, and two vertical-component geophone tools located at distances of several km from the injection point. In addition, a network of nine surface seismic stations, with 1 Hz vertical component geophones, was deployed at distances of several km from the injection point. All seismic data were recorded on analog magnetic tape, and digital data from the downhole geophones were obtained from about 1,800 seismic events during the 84 hours of seismic monitoring.

The water was injected in Precambrian granites and granodiorites. Seismic ray paths to the close-in (borehole) geophone tools were entirely within the granites; their seismic velocities were assumed to be homogeneous and isotropic (i.e. raypaths were assumed to be straight). In contrast, raypaths to the surface seismic stations, and, to a lesser extent, to the two more distant borehole instruments, were distorted by the lower velocity sediments that extend from the surface to a depth of about 700 m.

This paper discusses locational and fault plane studies of microearthquakes from experiment 2032. A companion paper (Fehler and Bame, 1985) discusses the source mechanics of microearthquakes from experiment 2032, as well as several earlier hydraulic fracturing experiments.

RESULTS FROM A DOWNHOLE SEISMIC NETWORK

Data from the five downhole instruments were used to obtain locations of seismic events by inversion of arrival times (P and/or S). Arrival times were picked from digital seismograms with a precision of 1 ms, which implies an optimum locational resolution of about 6 to 10 m. The seismic velocities used were obtained from detonator calibration experiments; the P velocity was 5.92 km/s and the S velocity was 3.50 km/s. Station corrections compensate for the slight observed variations from the assumed constant velocity. These station corrections were obtained from detonator calibration experiments and from a suite of well-recorded events scattered throughout the source volume. Individual station corrections are only a few percent of the travel times to the stations, and, hence, support the homogeneous-velocity assumption. The only exception is for one of the outlying borehole stations that was sited about 200 m above the granite-sediment interface, in a particularly low velocity formation. For this station, both P and S arrivals were considerably delayed relative to the assumed velocity, and the

travel time corrections are as large as 10% of the travel times. From the 1800 events that were digitized during the experiment, nearly 850 were located with computed locational errors of less than 50 m. These events are shown in the accompanying figures. We estimate that the precision of relative locations is 10-20 m and the uncertainty in absolute locations is 50-100 m.

We divide the time period of seismic monitoring into two segments. The first includes the period of injection, which lasted about 60 hours; the second comprises the initial 24 hours of venting. Figure 1 shows events from the injection period. The upper (left) frame is a map view of the activity. Although the seismicity does not define a simple planar distribution, the average strike of the seismic cloud is about N340^{0}E. Activity extends about 900 m in this direction. The upper (right) frame shows a vertical section view looking north (the projection plane is W - E). In this view, it is apparent that few events occurred within 100 m of the open-hole interval in target wellbore EE-3 (upper bold segment). Note that the seismic "cloud" is not vertical, but rather, dips about 75^{0} to the east, aligning sub-parallel to the two wellbores. Note also that the thickness of the seismic zone is about 150 m, which is considerably greater than the locational precision of 10 - 20 m. Hence, the thickness of the seismic zone is not an artifact of imprecise locations. In the lower (left) frame of Figure 1 is a vertical section looking to the west, i.e. onto the face of the seismic cloud. In this view, we see clearly the extent (about 800 m vertically and 900 m horizontally) to which activity spread away from the injection zone, as well as the heterogeneous distribution of activity within the stimulated region. Activity (and presumably fractures and/or opened joints) extended nearly symmetrically away from the injection zone.

Figure 2 shows seismicity in a "face-on" view (similar to that of the lower left frame of Figure 1) of events from the initial 24 hours of venting. The most important features to note in this plot are the lack of seismicity in the immediate vicinity of the injection (now venting) interval and the persistance of activity near the margins of the seismic cloud. In accord with the interpretation of Pearson (1981), the decrease of activity nearest the venting interval may result from rapidly decreasing pore pressure near the vent interval. Pore pressure remains high at greater distance from the vent zone, and hence, seismic activity continues there. Note also the concentration of activity to the upper right of the figure. Events within this concentration were some of the largest microquakes recorded during the experiment. Interestingly, the other area of relatively intense activity is at the lower left edge of the figure, at the opposite side of the seismic cloud.

The geometry of the seismic cloud as seen in Figure 1 is quite different from that reported in studies of previous experiments at Fenton Hill (e.g. Keppler, et. al., 1983). Seismic monitoring of previous experiments was limited to a single downhole triaxial geophone tool for close-in recording. Hence, events could be located only by use of the single-tool hodogram technique, which uses the particle motion of the incident P wave to obtain the direction from the seismic tool to the hypocenter, and the S minus P time to obtain the source distance. The particle motion is particularly sensitive to errors resulting from velocity heterogeneities and variations of the response of the tool components. Event locations obtained from arrival time information at several observation points are more robust than those from hodograms, even in the presence of velocity anomalies that result from creation and inflation of fluid-filled cracks. The major advantage of the hodogram technique is the limited number of observational boreholes and instruments that are required.

IMPROVED HODOGRAM LOCATIONS

In order to decrease the errors of the single tool hodogram technique, Keppler (1984) devised a method to utilize information from a second close-in triaxial geophone tool. In concept, this method uses hodograms at both triaxial tools and adjusts the mismatch of the incidence direction at each instrument. Hence, it should provide a more robust estimate of the event location than the single tool technique. In practice, this requires knowlege of the orientation of both instruments, a requirement not met in experiment 2032. As a compromise, hodogram information is taken from only one oriented tool (the symbol labelled by a 1 in Figures 1 and 2), and P and/or S arrival times are used from the both tools. We term this technique a partial double tool hodogram (PDH) method. Because of the intensive seismic monitoring of experiment 2032, this data set is the first to which the PDH technique has been applied. In essence, PDH places primary importance upon the tool-to-source distances computed from the S minus P travel time differences, and secondary importance upon the directional information. Hence, the straight line connecting the two tools is a prominent geometrical feature of this locational technique. The distances from the tools are fit exactly, so that radial and axial (relative to the line connecting the tools) control on the event location are quite strong. The azimuthal error is fully dependant on the P wave hodogram at the one oriented tool and is, therefore, the least well-constrained of the coordinates. The natural view for comparing locations from the PDH and arrival time techniques is that looking along the line joining the tools (Figure 3). The two tool positions in experiment 2032 were such that the orientation of the line joining them was nearly parallel to the

trajectories of the uncased sections of the two inclined wellbores, EE-2 and EE-3. The projection used in Figure 3 is nearly a view up and along the wellbores, and, in addition to juxtaposing results of the two location techniques, gives a vivid impression of how the fracturing failed to produce a connection between the wells. Note that the overall distributions of the locations are similar, although there is a suggestion that the PDH locations toward the edges of the cloud "wrap around" the line between the tools. This effect appears to be an artifact of uncertainty in the (hodogram) directions to the events. The median distance between the two different locations for each event is 80 m, although locations for individual events are as far apart as 280 m.

FAULT PLANE SOLUTIONS AND REGIONAL STRESSES

Signals recorded at the nine surface stations and at the two outlying downhole stations were used to study the focal mechanisms of as many events as possible. From the more than 700 microearthquakes detected at one or more surface stations during the experiment, a set of 69 of the larger events were chosen for studying focal mechanisms. In order to accurately determine take off angles to the various stations, the events had to be located. Unfortunately, data from the surface stations are difficult to correlate with data from the downhole stations. Therefore, the events studied were independently located from arrival times at the surface stations, using the joint event location-velocity determination technique of Crosson (1976).

First motions of all events studied show both compressions and dilatations and although the patterns of first motions showed great diversity, they are all consistent with shear slip fault plane solutions. From the set of 69 events, there were enough first motion data to obtain well-constrained fault plane solutions from only 26. Individual solutions were determined by the maximum likelihood method of Dillinger, et. al., (1972). Of the 26 events, 19 have fault plane solutions that are consistent with one of two typical solutions. The circles plotted in Figure 4 indicate the locations of these 19 events. The spread in epicenters seen in Figure 4 is comparable to that shown in Figure 1 (top left). Locations of events comprising solutions 1 and 2 are, in fact, intermingled within the entire distribution of events (although Figure 4 shows only a two dimensional view). The two typical fault plane solutions are shown in Figure 5. Note that the difference between the two solutions results entirely from a difference in first motion at a single station (this station plots in the southeast quadrant of the two solutions).

Both solutions have in common a near-vertical nodal plane that strikes almost N - S. Recall that the strike of the seismic cloud in Figures 1 was about 340° and the dip about 75° east. The nodal plane that the two solutions have in common is sub-parallel to the orientation of the seismic cloud, which suggests that it may be a dominant fault plane of the microearthquakes and that the earthquake fault surfaces may be en echelon. In addition, the T axes for the two solutions shown in Figure 5 trend roughly E - W, and are in reasonable accord with the regional stress observations of Aldrich and Laughlin (1984). The two solutions of Figure 5 are almost identical to composites obtained by Cash, et. al., (1983; note that they plot upper hemisphere projections) although they found the two solutions from two different experiments that were separated by about 1 km from each other. They proposed a spatial difference in the stresses associated with the nearby Valles Caldera complex as a possible explanation for the dramatic difference in slip direction indicated by the two fault plane solutions. It is clear that events comprising the two fault plane solutions from experiment 2032 are not spatially separated, and therefore their difference cannot be attributed to spatial differences in the stress effects of the nearby caldera.

GROWTH OF SEISMIC VOLUME

The "cloud" of microearthquakes appears to have expanded rather monotonically during the injection period. In order to quantify this growth, the seismically activated volume, V_s, was computed for various times during the injection phase of experiment 2032. From simple geometric considerations, V_s and V_{inj} can be related as: $V_s = (V_{inj}/c)^{1/n}$. The value of n in this relation provides insight into the way the fracture system grows with increased injection volume. Murphy, et. al., (1983) discuss what they term "planar" fracture growth (n = 2/3), in which only a few discrete fractures accommodate the injection volume, and "volumetric" fracture growth (n = 1), in which a larger number of relatively less open fractures accommodate the injection volume. Murphy, et. al., (1983) compiled V_s and V_{inj} data from a number of hydraulic fracture experiments world-wide, and argued that the data fit the "planar" model better than the "volumetric" model. Figure 6 shows a log-log plot of V_s and V_{inj} values from experiment 2032. From a least-squares fit to the data points, we obtain values of n = 0.9 and c = 1.9 X 10^{-3} (this relation is shown as the bold line in Figure 6). Hence, in contrast to the conclusions of Murphy, et. al., (1983), it appears that fluid injection during experiment 2032 produced a fracture system that is primarily volumetrically distributed.

CONCLUSIONS

Intensive seismic monitoring of a massive hydraulic fracturing experiment carried out at Fenton Hill, New Mexico has provided a view of the fracture system unobtainable by other techniques because of the 3.5 km depth at which the fracturing took place. The seismic results reported above show the potential of seismic information for characterizing the geometry, the state of stress, and the gross rock-hydraulic behaviour during the generation of an artificial geothermal reservoir. Specific findings for the reservoir created during experiment 2032 were:

-The finite thickness of the zone of seismicity and its spatial growth imply the creation of a zone of fracturing or joint stimulation, rather than a single classical fracture.

-First motions of all events studied from surface network data are compatible with shear slip, suggesting that any tensile or oscillatory source mechanism may only generate very weak seismic signals.

-Since the orientation of a focal plane that is present in most of the observed solutions is similar to that of the seismic volume, it may represent a predominant joint orientation.

-The agreement in overall distribution of locations for the same events using a travel time and the PDH technique is encouraging, and suggests that the latter is worth refining further.

ACKNOWLEGEMENTS

The Earth Science Instrumentation Group designed and fielded the seismic instrumentation with the dedication needed to acquire the data reported here. R. Kranz provided assistance with data analysis.

REFERENCES

Aldrich, M.J., and Laughlin, A.W., 1984. A model for the tectonic development of the southeastern Colorado Plateau boundary. J. Geophys. Res. 89, 10207-10218.

Cash, D., Homuth, E.F., Keppler, H., Pearson, C., and Sasaki, S., 1983. Fault plane solutions for microearthquakes induced at the Fenton Hill Hot Dry Rock Geothermal Site: Implications for the state of stress near a quaternary volcanic center. Geophys. Res. Lett. 10, 1141-1144.

Crosson, R.S., 1976. Crustal structure modeling of earthquake data, 1. Simultaneous least squares estimation of hypocenter and velocity parameters. J. Geophys. Res. 81, 3036-3046.

Dillinger, W.H., Harding, S.T., and Pope, A.J., 1972. Determining maximum likelihood body wave focal plane solutions. Geophys. J. R. astr. Soc. 30, 315-329.

Fehler, M., and Bame, D., 1985. Characteristics of microearthquakes accompanying hydraulic fracturing as determined from studies of spectra of seismic waveforms. Trans. Geoth. Resources Council 9 (this volume)

Keppler, H., Pearson, C.F., Potter, R.M., and Albright, J.N., 1983. Microearthquakes induced during hydraulic fracturing at the Fenton Hill HDR site: The 1982 experiments. Trans. Geoth. Resources Council 7, 429-433.

Keppler, H., 1984. Hypocentres of hydraulically induced microearthquakes obtained by a double tool hodograph method. EOS, Trans. Am. Geophys. Un. 65, 1011.

Murphy, H.D., Keppler, H., and Dash, Z.V., 1983. Does hydraulic fracturing theory work in jointed rock masses? Trans. Geoth. Resources Council 7, 461-466.

Pearson, C.F., 1981. The relationship between microseismicity and high pore pressures during hydraulic stimulation experiments in low permeability granitic rocks. J. Geophys. Res. 86, 7855-7864.

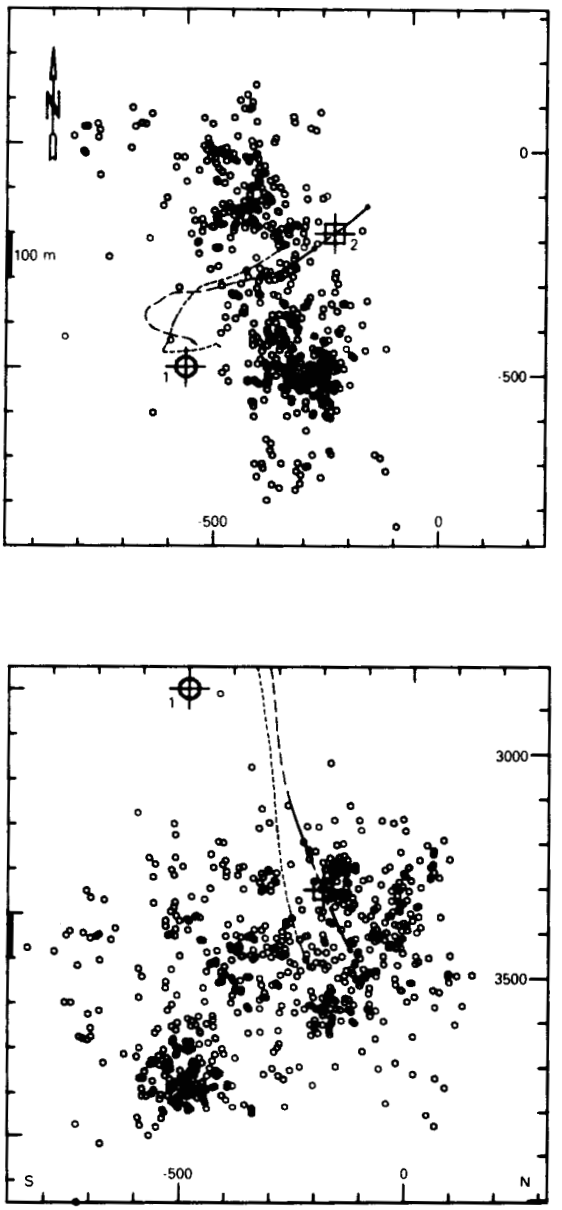

Figure 1: Plots of microearthquakes located by the network of downhole instruments during the injection phase of exp. 2032. Numbers are: 1: location of seismic tool in well EE-1; 2: location of seismic tool in well EE-3 (the third close-in tool was located about 425 m above tool 1). Bold portions of wellbore trajectories are open hole intervals in wells EE-2 (lower well; this was the injection well) and EE-3. The top left frame is a map view; the top right frame is a W-E vertical section (looking north); the bottom left frame is a S-N vertical section (looking west). Coordinates are in m relative to the tool in EE-1 (left and upper axes) and in m relative to a site survey reference point (right and lower axes), the depths in the section views are below surface.

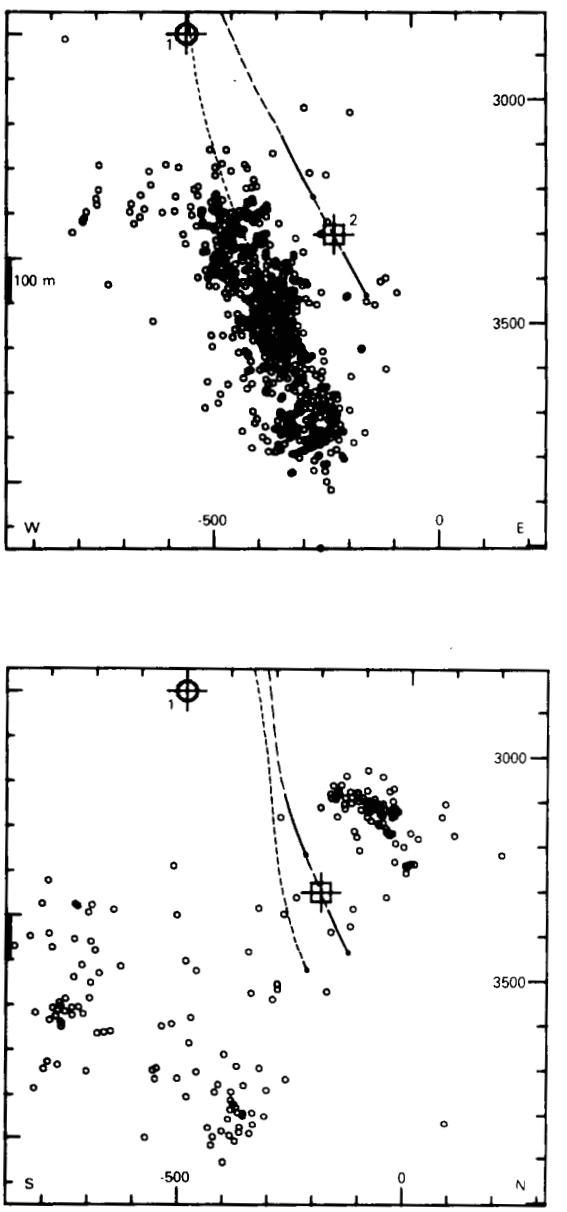

Figure 2: Plot of microearthquakes from the initial 24 hours of venting. The plot is a vertical cross section, with the view to the west, as in bottom left frame of Figure 1.

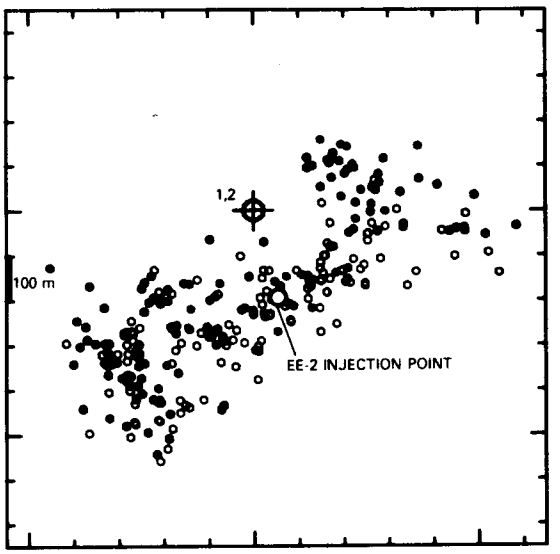

Figure 3: Inclined cross section showing arrival-time (open circles) and hodogram (solid circles) locations of 159 events. View is looking upward from the seismic tool in well EE-3 toward the tool in well EE-1. Scale is same as previous figures.

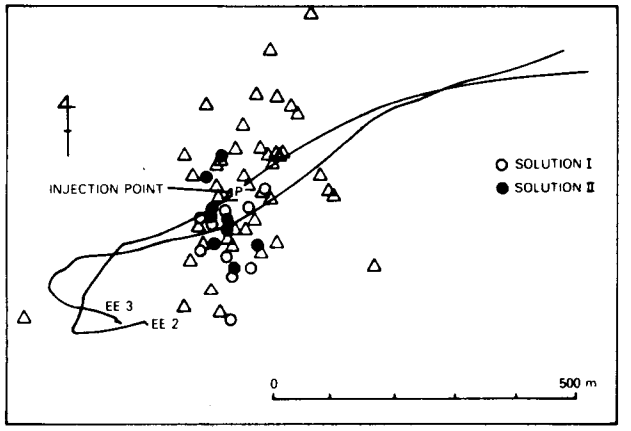

Figure 4: Map view of events located by the surface network. The circles are events for which fault plane solutions were obtained. Solid circles indicate events consistent with fault plane solution 1; open circles with solution 2.

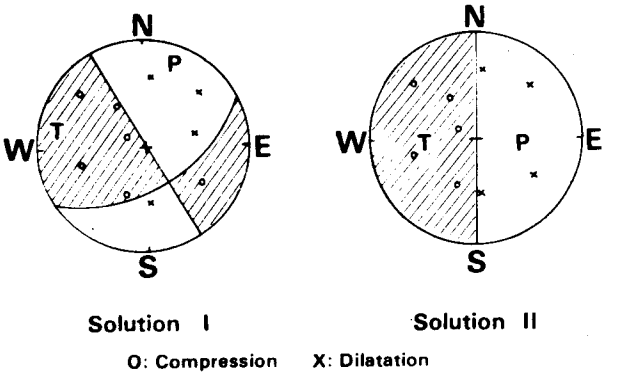

Figure 5: Composite fault plane solutions. Plots are lower hemisphere equal area projections.

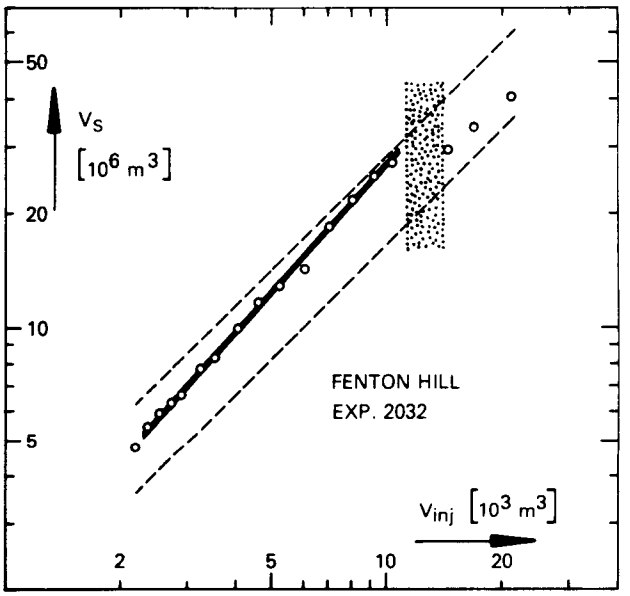

Figure 6. Plot of seismic volume V_s vs. total injected volume V_{inj}. The dashed lines indicate constant induced porosities of 3.5×10^{-4} (upper) and 6.0×10^{-4} respectively, which are upper and lower bounds from the data plotted. The solid line is a least-squares fit to the data points (see text). The stippled region indicates the time duration of a gap in the seismic data.